EASR

Engineering and Applied Science Research

https://www.tci-thaijo.org/index.php/easr/index

Published by the Faculty of Engineering, Khon Kaen University, Thailand

Convective systems observed by ground-based radar during the seasonal march of Asian summer monsoons in the middle of Thailand

Nattapon Mahavik*[1)] and Sarintip Tantanee [2, 3)]

[1)]Department of Natural Resources and Environment, Faculty of Agriculture Natural Resources and Environment, Naresuan University, Phitsanulok 65000, Thailand
[2)]Department of Civil Engineering, Faculty of Engineering, Naresuan University, Phitsanulok 65000, Thailand
[3)]Centre of Excellence on Energy Technology and Environment, Naresuan University, Phitsanulok 65000, Thailand

Received 29 March 2019
Revised 27 June 2019
Accepted 9 July 2019

Abstract

Understanding the characteristics of clouds is essential to support disaster mitigation and improvement of cultivation planning. Convective systems (CS) are a major contributor to the total number of rain systems over the tropics. In this study, the spatio-temporal characteristics of CSs extracted from instantaneous ground-based radar observations in Phetchabun, in central Thailand, were investigated during the seasonal march of Asian summer monsoons from July to September of 2010. The Open Source Library for Weather Radar Data Processing (Wradlib) was used to create gridded radar reflectivity at instantaneously observed times at a constant altitude of 3 km above the mean sea surface level. The geometric properties of the largest CS, such as echo size, fitted ellipse, and centroid, were also extracted and analyzed by applying the OpenCV library in a Python environment. CS classification produces two classes of CSs based on their speed, stationary and propagating. Propagating CSs are most frequent in August, accounting for 20% of the total number. Additionally, the propagating CSs in August cover relatively larger areas and produce stronger radar echoes than others, while stationary CSs in August have relatively more elongated forms. Classifying CSs based on direction, previous instantaneous scans show that the westerly class dominates across the study area, especially in August. Moreover, the westerly class is associated with stronger radar echoes compared to the easterly class. Additionally, the average speed of the easterly class has a tendency to decrease toward the end of the rainy season. The hot spot area with regard to CS severity has been identified as being in the southwest part of the study area.

Keywords: Convective systems, Ground-based radar, Hot spot analysis, Classify moving rain systems, Thailand

1. Introduction

The present characteristics and variability of precipitation systems must be known to understand future climate change [1]. However, it has become clear that global climate models are unable to effectively capture mesoscale rainfall characteristics. The rainfall amounts of the inland tropics are almost entirely influenced by mesoscale convective systems (MCSs) [2]. There have been several research studies focusing on MCSs from field observations and simulation models over the mid-latitude regions and tropics. They were reported with the use of radar, satellite observations and field experiments [2-6]. However, when it comes to the inland of the Indochina Peninsula (ICP), there have been very few studies of the characteristics of mesoscale precipitation systems. Therefore, the current study focuses on the characteristics of convective systems in the center of the ICP during the rainy season.

Based on observations over South Asia from the Tropical Rainfall Measuring Mission (TRMM), a large mountain range in South Asia is a key factor in the formation and behavior of precipitation systems in the region [7]. Near the mountain range, the convective clouds are small in size and weak intensity. Farther east, along the foothills, systems are more stratified. Storm morphology characteristics result in regional differences in rainfall modes. Nesbitt et al. [2] applied an ellipse-fitting technique to TRMM PR near-surface reflectivity to better understand storm morphology. Additionally, Lang et al. [5] found that MCSs were responsible for up to 90% of rainfall in selected land regions. The application of the ellipse-fitting technique to ground-based radar has also been used to document storm morphology characteristics in the southern Gulf of California [5]. The study focusing on the characteristics of convective clouds was done in India, which is located in the Asian summer monsoon region [8]. This is done to understand precipitating clouds over rain-shadow regions of

*Corresponding author.
Email address: nattaponm@nu.ac.th
doi: 10.14456/easr.2019.36

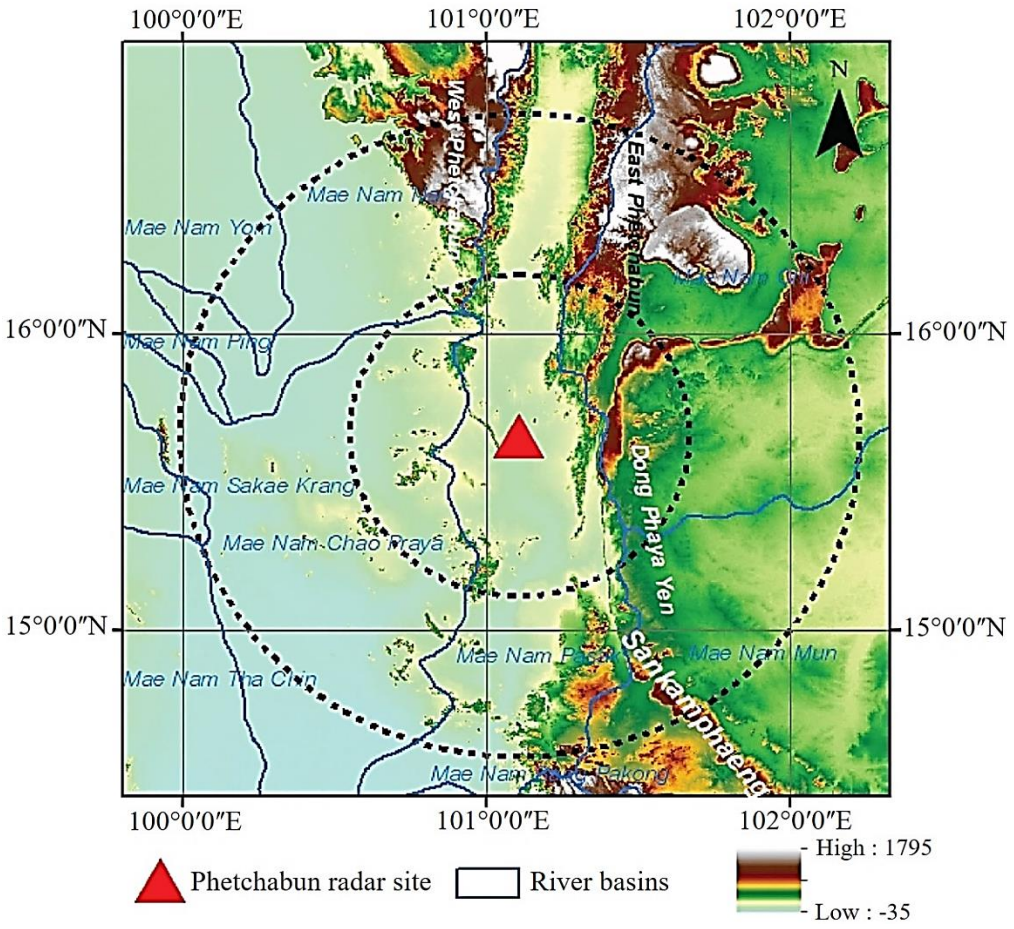

Figure 1 Map of the study area within range of the Phetchabun radar (represented as a triangle) at a radii of 60 and 120 km, represented as dash lines. The boundary of river basins under the radar observation area is represented as blue lines.

India, using only one season of radar data in the C-band mode. Additionally, the results of a study of cloud characteristics based on the 2D background classification method of Steiner et al. [9] has been useful for planning cloud seeding over drought-hit regions of India.

Understanding precipitation systems is essential for cultivation planning and disaster mitigation in the developing countries located in the ICP. The complex terrain in the ICP plays a critical role in rainfall patterns and characteristics [10]. The ICP is a tropical region influenced by both prevailing easterly and westerly winds during the rainy season [11-13]. The monsoon break during the seasonal march of the Asian summer monsoons is notable in that the rainy season is divided into two periods due to the movement of the intertropical convergence zone [14]. Therefore, the forcing synoptic systems are major influences on mesoscale precipitation systems over the central ICP.

Studies on the characteristics of precipitation systems at the mesoscale at ranges of 100-1,000 km are very limited in the center of the ICP. Satomura [15] used a two-dimensional, non-hydrostatic and cloud-resolving numerical model to simulate squall lines triggered over the extrusion of strong southwesterly prevailing winds during the rainy season. His results correspond to geostationary satellite images that showed persistent diurnal propagating precipitation in this region. These were responsible for maximal rainfall during evenings and nights, which corresponded to previous observations [12, 14, 16]. However, the spatio-temporal characteristics of the CSs have not been well described during the seasonal march of the Asian summer monsoons in the central ICP. Ground-based radar is one of the methods of fine-resolution observation that can reveal the spatial and temporal structure of MCSs. Therefore, in this study, the authors intended to describe the characteristics of the largest CS influencing spatial rainfall patterns over the area of radar coverage of the Phetchabun radar station, Thailand, which is in the middle of the ICP. Additionally, spatial clustering of the CSs was investigated to identify locations across the study area where the most severe weather systems are found. The ellipse-fitting technique has been applied to find the geometry of CSs to enhance the analysis of precipitation systems.

This paper is organized as follows: The study area and radar data are described in Section 2. Section 3 presents analysis of precipitating cloud types and spatial hot spots. Section 4 provides the results and discussion, and Section 5 gives a summary.

2. Study area and radar data

In this study, radar echo data from the weather radar operated by the Thai Meteorological Department (TMD) was used. Data was gathered by Phetchabun Radar, located in central Thailand (Figure 1) at the geographic coordinates of 15° 39′ 24″ N and longitude 101° 6′ 29″ E. It is located among important Thai river basins such as Pasak, Nan, Yom, Chao Phraya, Mun and Chi. Situated on a plain of the Pasak river basin, the radar is installed on a tower, 74 meters above the mean sea level (MSL). It is capable of

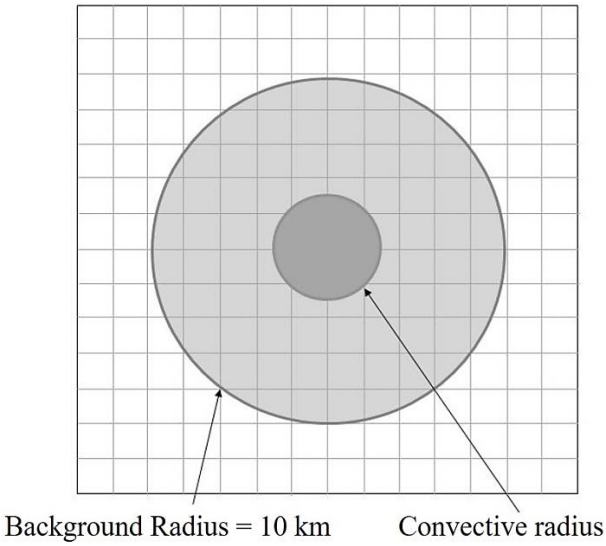

Figure 2 Schematic diagram of convective grid points adopted from Steiner et al. [9]. The lightly shaded circular area indicates the area within the background radius surrounding a given grid point. The darker-shaded area represents the area around the convective center, if identified as such, it is included as convective area. The radius of this convective area is a function of the average reflectivity within the background radius.

observations up to a range of 240 km in the C-band frequency at a resolution of 500 meters with a beam width of 1 degree. Scanning occurs continually at a rate of three scans per hour, at 00, 30 and 45 minutes after the hour, with the volume scanning mode of 10 elevation angles (0.0°, 1.3°, 2.9°, 4.9°, 7.3°, 10.2°, 13.8°, 18.2°, 23.5°, 30.0°).

Since the radar site is surrounded by mountainous ranges to the west, east and southwest, i.e., the West Phetchabun, East Phetchabun, and Dong Phraya ranges, respectively, the lower radar beam is shielded by the surrounding mountain ranges due to beam blockage. Therefore, in this study, the observation ranges have been limited to a range of 120 km, which is sufficient for the task of observing the rain systems over the radar coverage area. The current study involved analysis of 6,233 files compiled over three months (July – September of 2010) in a portion of the rainy season on the ICP. This huge volume radar scans required considerable data manipulation to do an effective spatio-temporal analysis for rain system classification.

In order to observe the rain systems near the lower troposphere, a constant altitude plan position indicator (CAPPI) at an altitude of 3 km above MSL was constructed as a radar reflectivity map in dBZ units at a horizontal resolution of 1 km. A CAPPI was created for each instantaneous radar scanning time using an open source library for manipulating the radar data written as a Python script in the Open Source Library for Weather Radar Data Processing (Wradlib) [17]. Radar reflectivity, in the form of a raster grid map, was easily manipulated and analyzed using a geographic information system.

3. Methods

a. Classification of precipitating clouds

An automated method to classify CSs from a huge dataset of radar volume scans is required to obtain an objective result of the largest CSs from an instantaneous radar scan. In the algorithm portion of CS separation, the CS extraction developed by Steiner et al. [9] (as shown in Figure 2) was adopted and implemented in a Python script. A mean background reflectivity curve was developed by Steiner et al. [9] to differentiate between convective and stratiform clouds. This curve represents the difference between the reflectivity at a grid point and background reflectivity, which must be exceeded for the grid point to be designated as a convective center. The curve is given by:

$$\Delta Z = \begin{cases} 10, & Z_{bg} < 0 \\ 10 - Z_{bg}^2/180, & 0 \le Z_{bg} < 43 \\ 0 & Z_{bg} \ge 43 \end{cases} \quad (1)$$

where ΔZ is the difference between reflectivity at a grid point in decibels and radar reflectivity (Z_{bg}) in *dBZ*. The reflectivity difference of a given radar echo must exceed the background intensity following the peak criteria curve in Figure 7 of Steiner et al. [9]. This cloud classification scheme has been widely used in research in other monsoon regions, including India [8]. Naturally, the convective and stratiform rain types differ in physical characteristics, including their structure, intensity, and microphysics. Therefore, a radar echo at a height of 3 km with resolution at 1 km was used to separate convective areas from the background echoes in dBZ. To avoid bright band signatures from stratiform clouds, the CAPPI radar is limited to a range of 120 km at an approximate altitude of 3 km. The horizontal intensity of radar echoes was simply used to detect the initial center peak of minimum a CS at 43 dBZ of radar reflectivity. This was done to separate CSs from background echoes [18-19]. After the initial convective center peak was detected, a circular shape with a radius of 10 km was applied using the convective center peak as its center point. An equation developed by Steiner et al. [9] was used to check whether the pixels surrounding the center were convective or not.

Based on the intensity of horizontal reflectivity (Figure 3a), the radar echoes during the MCS overpass of the study area were classified into two types, convective and non-convective (Figure 3b). The implemented program as a Python script can classify both types of radar echoes from

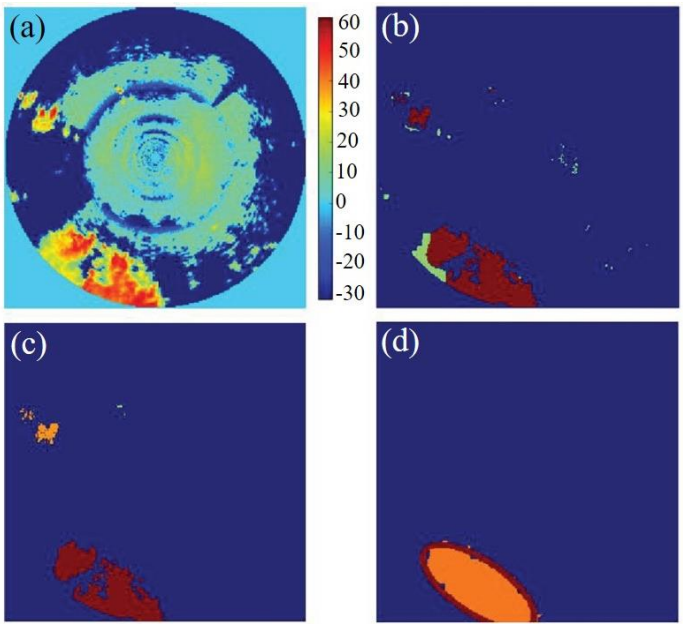

Figure 3 Classified rain cloud types on September 3, 2010 at 13:00 (a) original radar reflectivity shown in dBZ (b) classified convective and stratiform clouds, shown as red and green colors, respectively (c) classified convective clouds shown in different colors and (d) the fitted ellipse superimposed on the largest convective cloud after application of smoothing kernel.

the CAPPI created from the volume scan mode during the whole observation period. This study focuses on understanding the characteristics of the largest CS appearing during instantaneous radar scanning. The algorithm to detect the CS is implemented using the OpenCV library [20].

OpenCV, an open source library for digital image processing, is accessed using a Python script to delineate the convective area and non-convective precipitating clouds (Figure 3c). After detection of the largest CS, the fitellipse function in OpenCV is applied to the CS to realize its ellipse aspect ratio through major and minor ellipse axes (Figure 3c). Before application of the fitellipse function, the closing morphology function in OpenCV, MORPH_CLOSE, is applied with a 10 x 10 km kernel to eliminate the small holes inside the foreground objects. If the ratio between major and minor ellipse (hereafter ratio) is differs significantly from 1.0, the shape of the CS is a more elongated in form.

Since the ellipse axes are extracted from a fitted ellipse, the centroid and area of the fitted ellipse for each radar instantaneous scan is also extracted to further investigate the CS characteristics. The propagating criteria of the CS are set using the extracted information from the fitted ellipse of the CS to classify whether it is of the propagating or stationary class. The overlapping percentage of the ellipse area and propagating speed of the CS, based on a centroid between the particular CS of the present radar scan and the three previous radar scans, is calculated. A CS is a propagating CS when the overlapping percentage and propagating speed of the CSs exceeds 50% and 1 m s^{-1}, respectively.

b. Hot spot analysis

To evaluate the spatial cluster of the convective centroids, Hot Spot Analysis (Getis-Ord Gi*) is done based on [20] using the Hot Spot Analysis function in ArcGIS. A convective centroid must have a high value and be surrounded by other centroids with high values of radar reflectivity to be identified as a statistically significant CS hot spot. The Getis-Ord local statistics are given as:

$$G_i^* = \frac{\sum_{j=1}^{n} w_{i,j}x_j - \bar{X}\sum_{j=1}^{n} w_{i,j}}{S\sqrt{\frac{[n\sum_{j=1}^{n} w_{i,j}^2 - (\sum_{j=1}^{n} w_{i,j})^2]}{n-1}}} \quad (2)$$

$$\bar{X} = \frac{\sum_{j=1}^{n} x_j}{n} \quad (3)$$

$$S = \sqrt{\frac{\sum_{j=1}^{n} x_j^2}{n} - (\bar{X})^2} \quad (4)$$

where x_j is the convective centroid feature attributing value for the convective feature j, $w_{i,j}$ is the spatial weight between convective systems i and j, and n is equal to total number of convective features. The G_i^* statistic is a z-score. No further calculations are required.

The Getis-Ord local statistic [21] was applied to the detected CS centroid dataset to detect hot spot (cold spot) areas where statistically significant hot spots (cold spots) are located. Each of the CS centroids were calculated using the Gi* statistic, as shown in equation (2), which will return z-scores and a p-value. The resultant z-scores and p-values identify where convective centroids, with either high or low values of radar reflectivity cluster spatially. The statistically significant positive or negative z-scores of the CS centroid mean that the relevant CS is surrounded by CSs of relatively larger or smaller values.

c. Easterly and Westerly Classifications

During the boreal summer monsoon march, the ICP is affected by the interconvergence zone of two main wind systems, which are southwesterly and easterly from the western North Pacific (WNP). The MCS characteristics

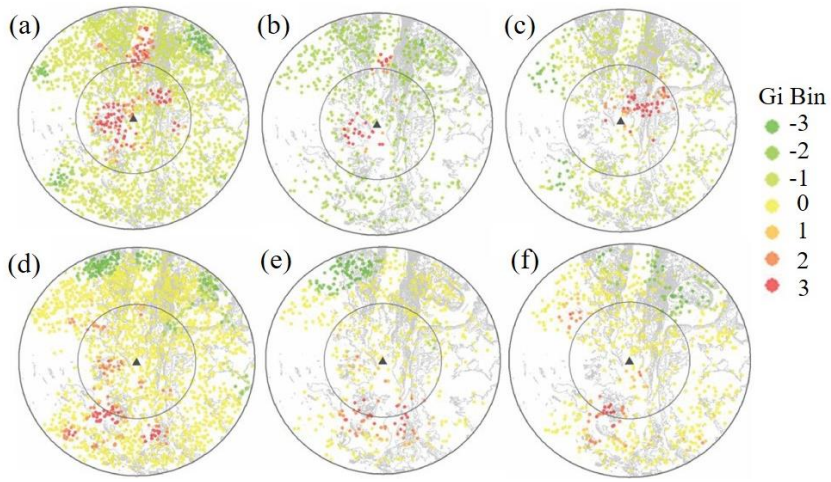

Figure 4 Hot spot analysis of the largest convective clouds from July to September 2010 (a-c) hot spots of areas for all centroids, propagating and stationary classes (d-f) hot spots of echo intensity for all centroids, propagating and stationary classes. Contour lines shown in gray represent elevation at interval of 100 meters. The triangle represents the location of the radar station. Radar observation ranges are represented in circles at distances of 60 and 120 km from the radar station. Gi bin is the groud of z-scores calculated from Gi^* shown in equation 2.

Table 1 Overall statistics for the convective clouds

	Mean	**Standard Deviation (S.D.)**
Area (km^2)	1184.23	1650.59
Speed ($m\ s^{-1}$)	9.58	7.75
Ellipse shape	1.99	0.83
Echo intensity (dBZ)	54.29	5.31

generated over the study area by these two synoptic wind sources need to be well understood. The westerly and easterly classes of CSs were classified in this study through the use of radar capabilities. First, after the centroid of each CS was detected, the bearing azimuth where the radar echo originated was derived for each pair of considered radar scans, as well as the previous three instantaneous scans.

Next, the average of bearing azimuths for these three pairs of radar scans was calculated. Determination of the average bearing azimuth was carried in eight meteorological directions. Finally, the majority of the meteorological directions were obtained and used for each scan in the analysis.

4. Results and discussion

a. Overall characteristics of convective systems

The overall characteristics of the CSs are summarized in Table 1. Average area of the CSs is similar to the echo sizes observed by Vientiane Radar, Lao PDR [22] during the boreal monsoon season on the ICP. However, the standard deviation (S.D.) shows a larger variation during the season march. Additionally, the CS's average speed also displayed large variations during the observation period. The strong radar echo in units of dBZ indicates reflectivity of the detected MCSs convective core. There has been a great deal of previous research on determining the minimum threshold in units of dBZ using convective reflectivity. In this study, we used the radar echoes at 43 dBZ as the minimum threshold to detect CSs, following the research of Steiner et al. [9]. Variation in surface heating is the main reason for mesoscale variation, as it causes more intense convection over the continents and large islands compared to oceans [23].

Taking a further step, the geometry of a fitted ellipse over a CS was used in CS shape investigation. Using the ratio between the major and minor axes of the fitted ellipse can describe the shape of a CS. If the ratio of the two axes of a fitted ellipse is near 1.0, the CS's shape is rather circular. Otherwise, it has a more elongated form. It was found that the elongated shapes were the most common in the study area during the studied seasonal monsoon march.

b. Propagating and stationary convective systems

CSs can be classified as one of two types, propagating and stationary, based on the propagation criteria discussed above and shown in Table 2. This is done to compare CS characteristics. Propagating and stationary class CSs were found in 2,120 and 1,816, instantaneous scans, respectively. The average area of the propagating class is larger than that of the stationary class. Furthermore, a larger variation in the size of the propagating CS area was noted compared to that of the stationary class.

Conversely, radar intensity, shown by dBZ, of the stationary class shows high variation compared to the propagating class. This finding may explain why the internal dynamics of MCSs during the evolution stage of the propagating class is more stable in rainfall intensity than that of the stationary class. Based on the fitted ellipse, the shapes of the two CS classes are generally the same.

To understand the distribution of spatial CSs, Hot Spot Analysis (Getis-Ord Gi*) [21] was applied to detected the locations of the CS. The spatial statistics in the clustered CS hot spots (cold spots) of the area indicate a concentration of high larger (smaller) area of CS centroids. It was found that clustered hot spot areas were located in the upper part of the study area, along the Pasak Basin (Figure 4a). Compared to hot spot areas of propagating CSs, the clustered hot spot areas of all CSs were largely influenced by the hot spot areas of the propagating convection (Figure4b) rather than

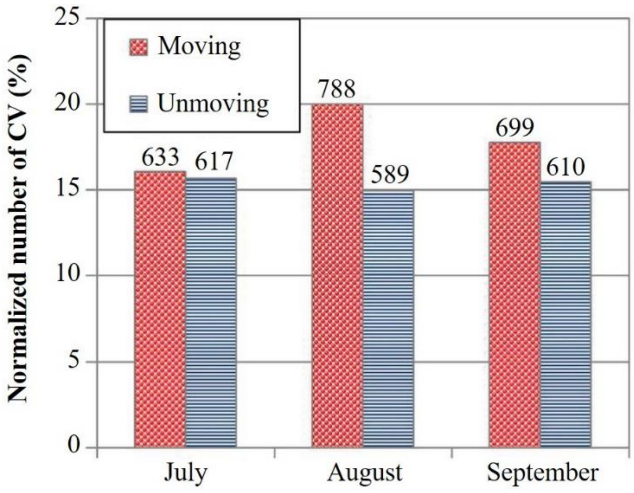

Figure 5 Normalization of the number of the largest convective clouds for both propagating and stationary class. The numbers above each bar indicate the total number of convective clouds for each class.

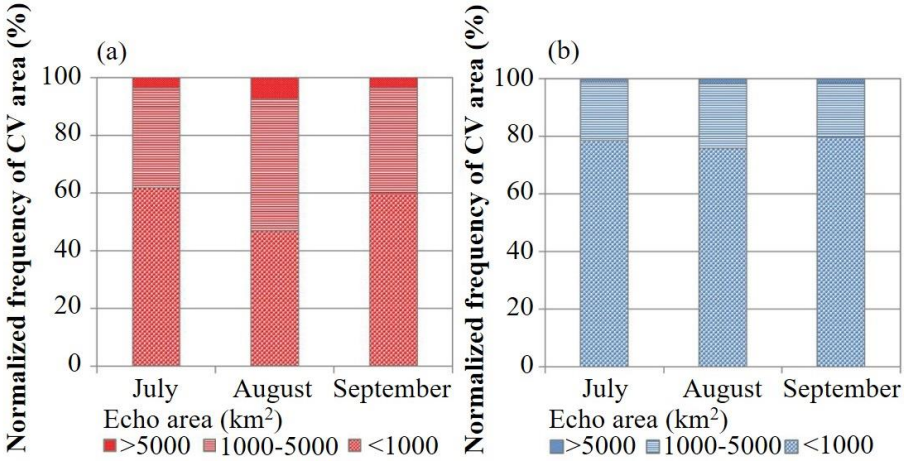

Figure 6 Normalization of frequency radar echo area of the largest convective cloud for both (a) propagating and (b) stationary classes.

Table 2 Overall statistics for propagating and stationary class

	Propagating class		Stationary class	
	Mean	**Standard Deviation (S.D.)**	**Mean**	**Standard Deviation (S.D.)**
Area (km^2)	1485.33	1838.03	832.53	1315.71
Ellipse shape	1.988	0.773	1.996	0.883
Echo intensity (dBZ)	55.33	4.59	53.07	5.82

those of the stationary convective system (Figure 4c). The spatial clustering of hot spots (cold spots) in the case of radar echoes was clearly delineated. Clustered stronger (weaker) radar echoes were detected in the lower (upper part) of the study area (Figure 4c). Specifically, the stronger and weaker radar echoes were generated by both propagating (Figure 4e) and stationary class CSs (Figure 4f) over the lower and upper parts of the study area, respectively.

Normalization of the area with respect to the total number of the CS scans is shown in Figure 5. This was done to understand the distribution of both propagating and stationary class CSs across the area during the seasonal march of the monsoon. The large number of propagating CS contributes to the total CS number during the observation period. Both the highest percentage of propagating CSs and the lowest percentage of stationary CSs occurred in August.

CS area has been classified into four levels during three months of the observation period. This was done to understand the contribution of the average areas of the CS for both propagating and stationary classes during the seasonal march. In the case of propagating CSs, small size CSs, at 1,000 km^2, dominated the observation area, except during August, when CSs of 1000-5000 km^2 were most prevalent, as shown in Figure 6a. Specifically, the sizes of the CSs found during August were relatively larger than those in other months. The stationary class, on the other hand, were relatively smaller in size and widely distributed in large proportion over the months of observing scanning radar reflectivity, as shown in Figure 6b.

c. The influence of propagating convective systems on easterly and westerly classes

In order to understand the contribution of the propagating CSs during the observed period, the frequency of propagating directions, that is, where radar echoes come from, are summarized in Figure 7. These are normalized

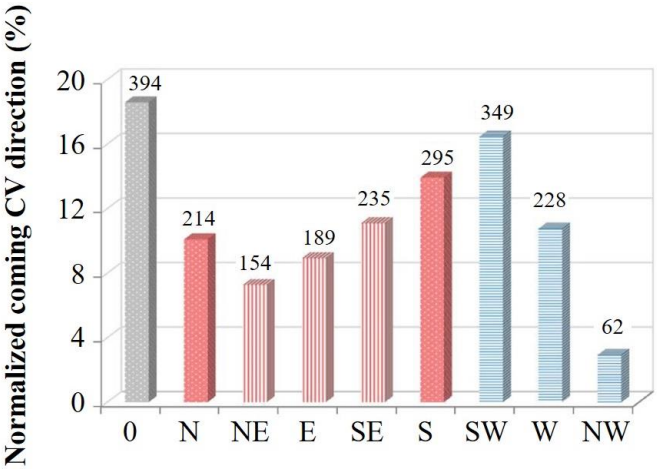

Figure 7 Normalization of the frequency of classified coming directions of the largest propagating convective cloud. "0" indicates unclear arrival direction (see text for details). The patterns of vertical and horizontal filled bars indicate easterly and westerly classes, respectively. The numbers above each bar indicate the total number of convective clouds for each class.

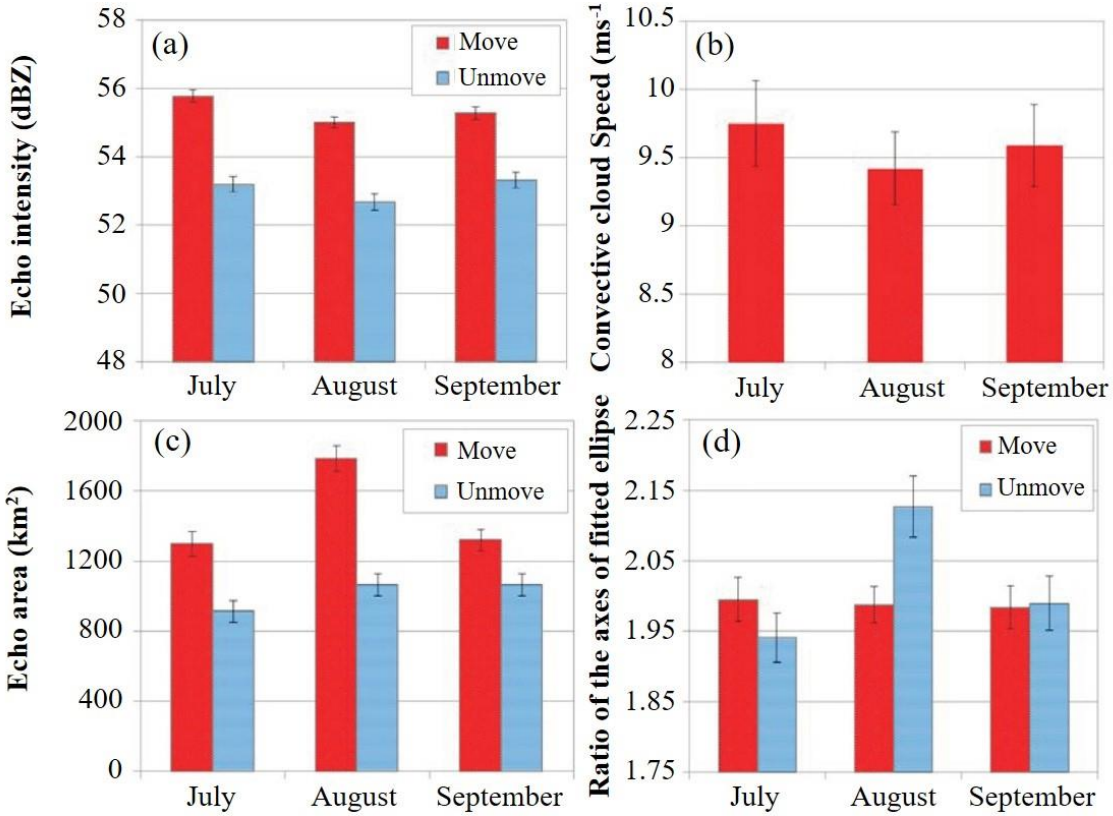

Figure 8 Characteristics of the largest convective clouds as propagating and stationary classes (a) echo intensity (b) moving speed of propagating class (c) echo area (d) ratio of the axes of the best fitted ellipse. Standard errors are represented by error bars.

with respect to the total number of convective clouds in the sample population. The largest number of echo arrivals from a particular direction identified during each one hour period was determined as the arrival direction for that hour. To observe an arrival direction of a CS, eight meteorological directions were used (1-8). The number and arrival directions of CSs observed during July-September, 2010 are shown in Figure 7. Unclear arrival direction is represented as direction 0, meaning that no single direction was identified by the count in a given hour. Although unclear direction of propagating class comprised the largest group, Figure 9 shows the result when the coming echoes were grouped into easterly and westerly directions. Here, the southwest direction is dominant, followed by south, and southeast. The wind directions were grouped into easterly and westerly by excluding southerly and northerly coming echoes to determine the influence of the two dominant wind directions. It should be noted that the resulting number is not the total number of CSs. Rather, it is the number of available instantaneous scans of the CS findings.

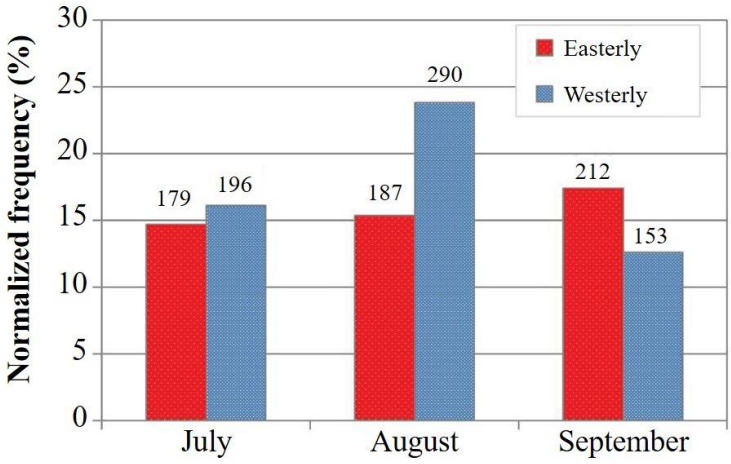

Figure 9 Normalized frequency of the two most dominant classified arrival directions of the largest propagating convective cloud. The numbers above each bar indicate the total number of convective clouds for each class.

Characteristics of the propagating and stationary classes of CS were investigated in a monthly comparison between the two classes (Figure 8). The propagating class was found to be stronger than stationary class in every month (Figure 8a). The strongest radar reflectivity was found in July for the propagating class, while found that the stationary class, it does not vary much from month to month. Additionally, the average area of the propagating CSs was found to be larger than that of the stationary class in every month. The largest area of the echo size in August varied among the propagating class CSs, while it did not much vary in the stationary class CSs by month (Figure 8c). Comparing the propagating class characteristics in this study with those of Satomura et al. [22], who used data from Vientiane Radar in the Lao PDR, it is found that the echo sizes of returning rain systems in July 2008 were relatively similar. However, investigation of the stationary class CSs in July 2010 provided additional information about MCSs that showed a difference in area.

In contrast to other CS characteristics, the shape of the fitted ellipse indicates high variation between the stationary and propagating classes by month. The stationary class in August shows the highest value of ratio of ellipse axes, which means a more elongated form (Figure 8d). The relatively unvarying form of the CSs in the propagating class corresponds to the propagating speeds of this class (Figure 8b).

The bearing (direction) of the returning echo was classified as either easterly and westerly as shown in Figure 9. This was done to understand the characteristics of the largest propagating convective system for each scan. The directions of NE, E and SE were grouped into easterly classes, while the directions of NW, W and SW were grouped into westerly classes. Investigation of these classes was separated into months and normalized with respect to the total number of convective cloud instances.

The largest total number of propagating class CSs occurred in August, indicating the dominance of the easterly class. An abrupt decrease in the number of propagating westerly class CSs was found in September, when an increase in the number of the easterly class CSs occurred. In the latter half of the monsoon season, disturbance from WNP dominates the ICP and introduces easterly rain systems during the second active period of the rainy season [24].

Radar echoes have shown different characteristics during seasonal march, as illustrated in Figure 10. In July, the elongated shape and relatively smaller size of the westerly class dominated the observations. Also, the echo intensity of the westerly class is usually stronger than that of easterly class, as shown in Figure 10a. Decreasing trends of average speed are found in the easterly class toward the retreat of the monsoon season, as shown in Figure 10b. Generally, the largest mean area size of the westerly class is found in August, as shown in Figure 10c. The westerly class provided the strongest radar echoes in all of the studied months. Furthermore, the strongest average radar echo appeared in the westerly class during August. In contrast to the average propagating speed, the average shape of the easterly class became a more elongated form, as shown in Figure 10d. Both convective lines with trailing stratiform precipitation and with leading stratiform precipitation have potential to create flash flooding [25]. Previously, Fritsch et al. [26] used radar and satellite data to detect the size of slowly propagating meso-vortices that triggered heavy rain with localized flash flooding in the mid-latitude regions of the United States.

d. Frequency of the convective systems in the easterly and westerly classes

Normalization of the total number of relevant characteristics of the easterly and westerly classes was done to understand the characteristics of propagating convective systems on the frequency of occurrence during the seasonal march of the summer monsoon, as shown in Figure 11. In general, the frequency of the smaller CSs of less than 1000 km^2 dominates over the period in both classes, as shown in Figure 11 (a-b). However, in August, CSs that were greater than 1,000 km^2 tended to dominate the area in both classes.

Generally, it is found that the ratio of the fitted ellipse ranges from 1.0-2.0 for both classes throughout the studied period, as shown in Figure 11 (c-d). In particular, this is mostly found in July for the easterly class, while it is primarily found in August for the westerly class. More elongated forms of the propagating class with fitted ellipses greater than 2.0 are found in August for the easterly class, while those elongated CSs are found in July for the westerly class. The more elongated CSs at a ratio of the fitted ellipse

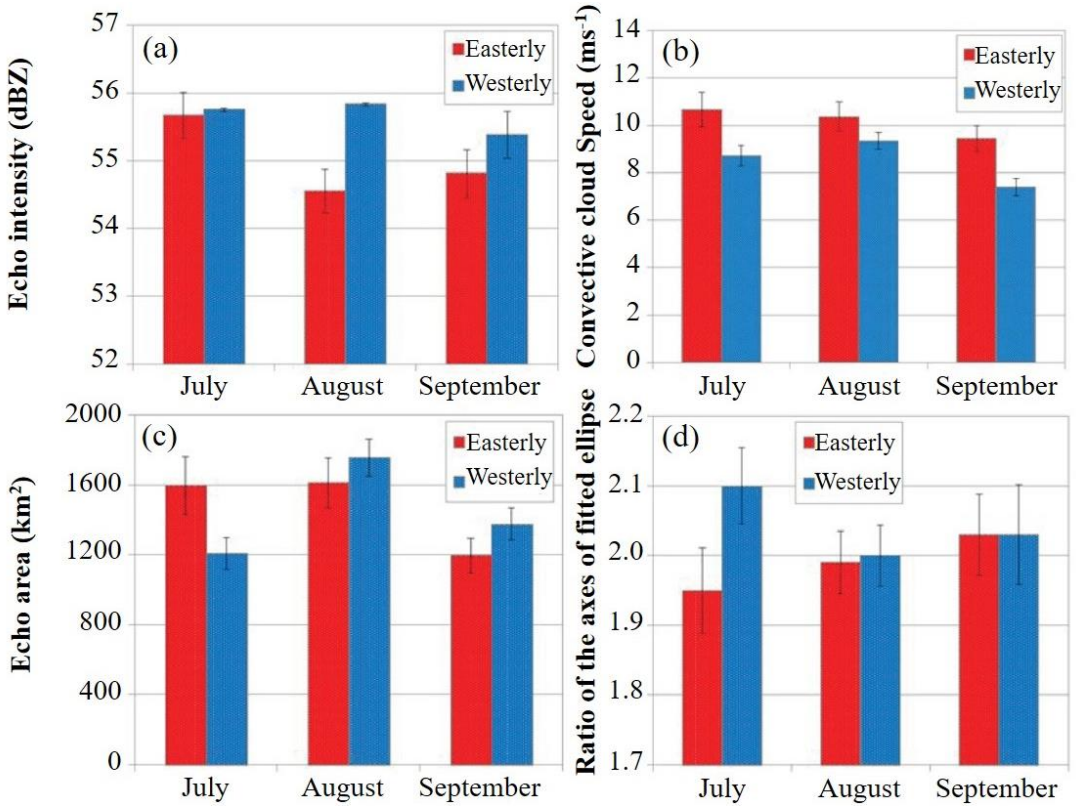

Figure 10 Characteristics of the largest convective clouds of the easterly and westerly classes (a) average echo intensity (b) average speed of convective cloud (c) area average of radar echo (d) average ratio of the axes of the best fitted ellipse. Standard errors are represented by error bars.

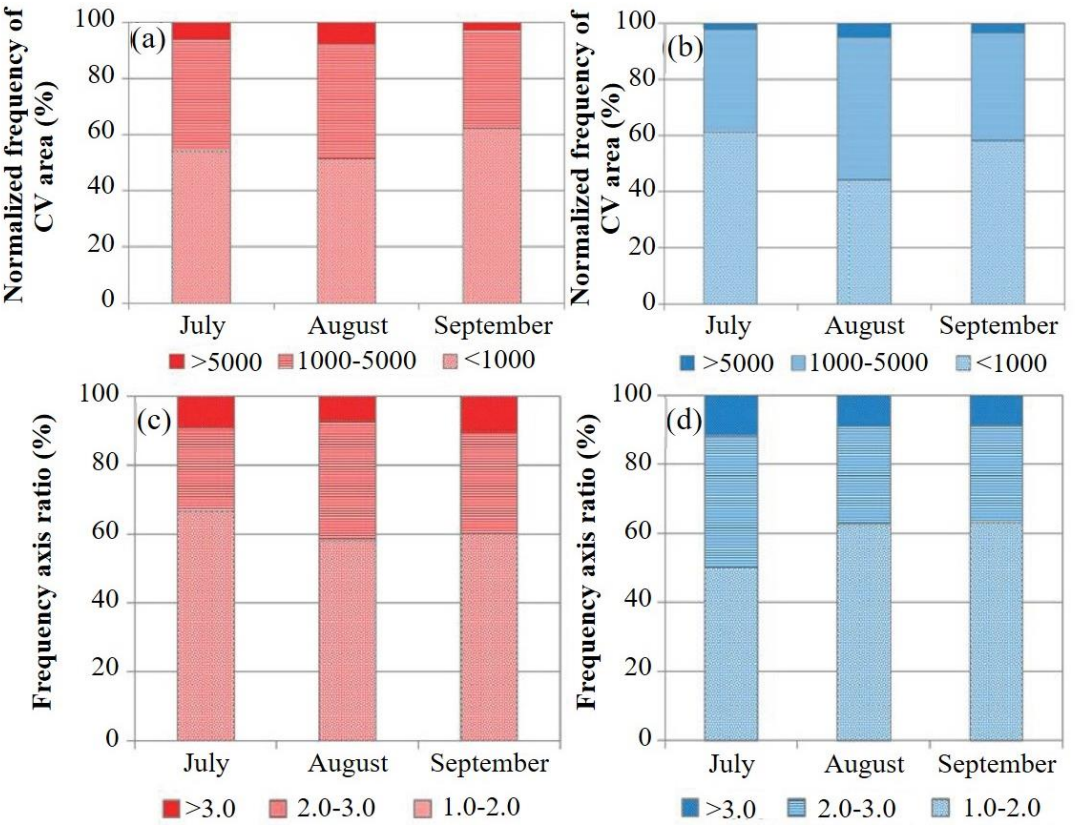

Figure 11 Normalized frequency of radar echo area for the largest convective clouds (a) easterly class, (b) westerly class. Normalized frequency of the axis ratio between major and minor axes of the fitted ellipse for the (c) easterly class (d) westerly class (see text for details).

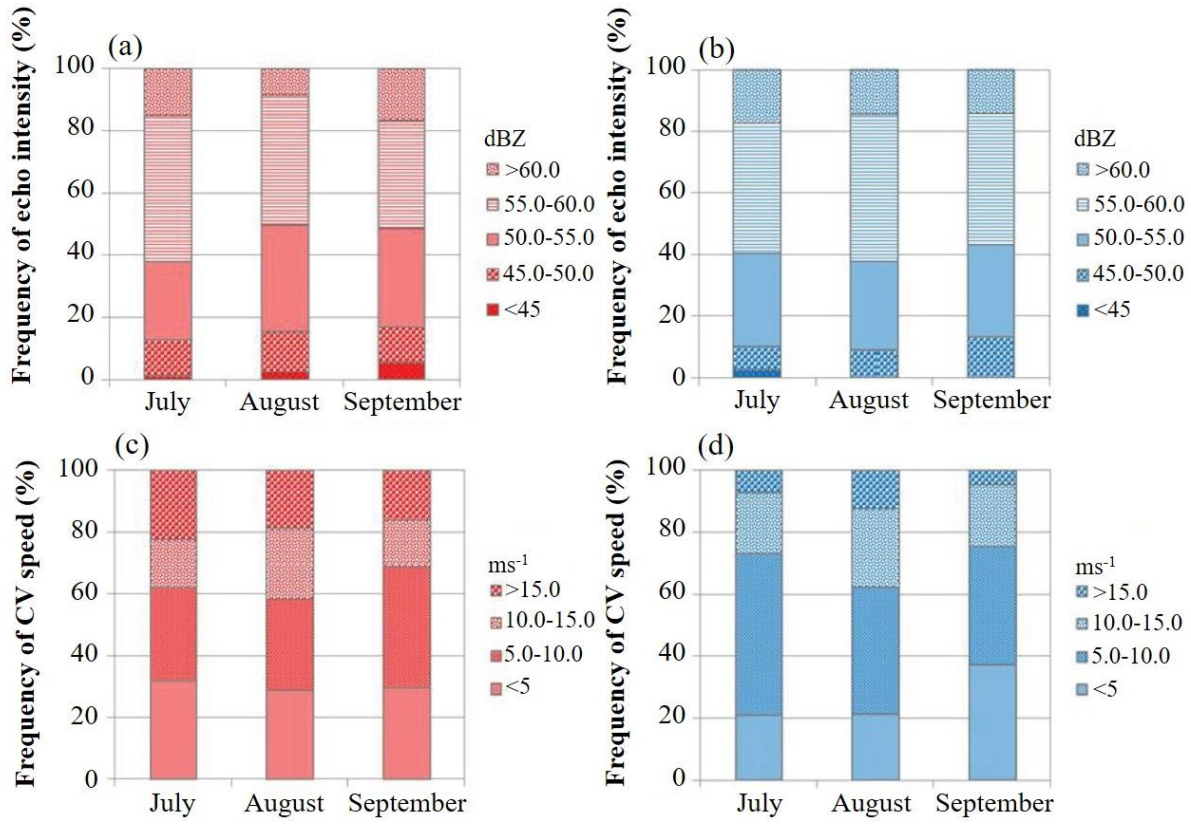

Figure 12 Normalized frequency of radar echo characteristics for the largest convective cloud (a) echo intensity of easterly class, (b) echo intensity of westerly class. Normalized frequency of the convective cloud speed (c) easterly class, (d) westerly class.

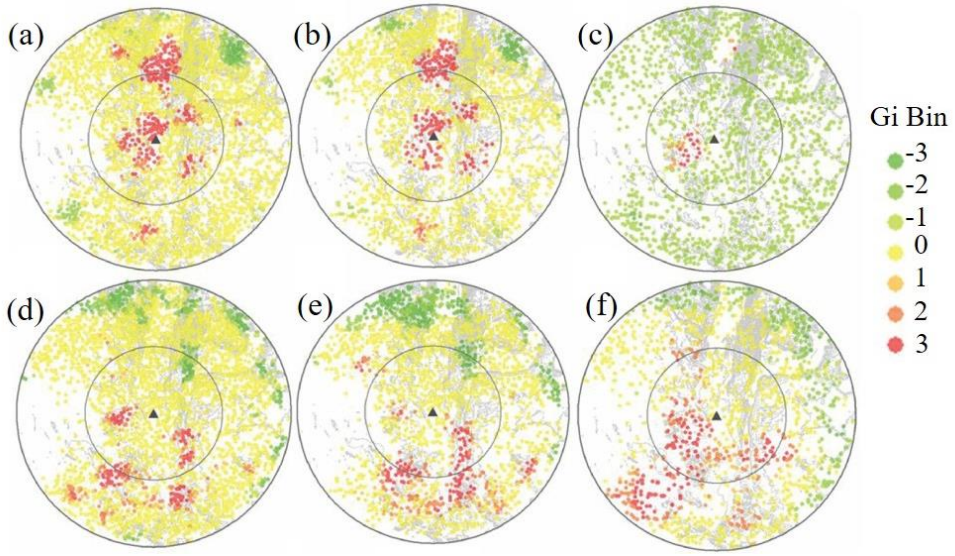

Figure 13 Hot spot analysis of the largest convective clouds from July to September 2010 (a-c) hot spot of echo area for all centroids, easterly and westerly classes (d-f) hot spot of echo intensity for all centroids, easterly and westerly classes. Contour lines represent elevation at an interval of 100 meters. Triangles represent the location of the radar station. Radar observation ranges are represented in circles at distances of 60 and 120 km from the radar station. Gi bin is a groud of z-scores calculated from Gi^* as shown in equation 2.

greater than 2.0 in westerly class decreased in frequency toward the end of September. Generally, strong radar echoes, greater than 55 dBz, were found to be the most common over the study area for all studied months, as shown in Figure 12(a-b). Specifically, stronger radar echoes were found more frequently in the westerly class than in the easterly class. The strongest radar echoes were found in July in the easterly class, and in August for the westerly class. Very strong radar echoes, greater than 60 dBZ, tended to decrease in frequency toward the end of September. In general, propagating class

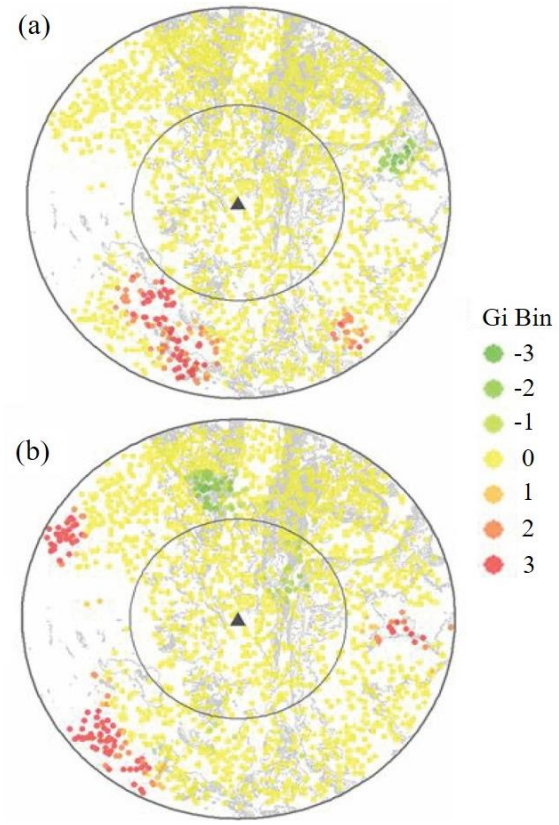

Figure 14 Hot spot analysis of the largest convective clouds in the case of a combination of easterly and westerly classes from July to September 2010 (a) hot spot of the ratio of the axes of the best fitted ellipse (b) hot spot of the speed of the convective cloud. Contour lines represent elevation at intervals of 100 meters. Triangles represent the location of the radar station. Radar observation ranges are represented in circles at distances of 60 and 120 km from the radar station. Gi bin is a groud of z-scores calculated from Gi^* shown in equation 2.

CSs with speeds of 5-10 ms^{-1} are frequently found in both classes, as shown in Figure 12(c-d). Remarkably, the frequency of CSs with speeds faster than 15 m s^{-1} decreases toward the end of September for the easterly class, while the frequency of those with speeds slower than 5 m s^{-1} increases toward the end of September for the westerly class.

e. Discussion

To understand the spatial distribution of the easterly and the westerly classes over the study area, we investigated the clustered CSs using hot spot analysis, as shown in Figure 13. The clustered size of the CS area shows hot spot areas in the center and upper parts of the study area (Figure 13a). Specifically, the center and upper parts of the area are covered with hot spots related to the easterly class (Figure 13b), while the westerly class hot spot area is located near the west side of the radar station (Figure 13c). When the data of both classes are combined, stronger radar echoes identify clustered areas in the south and southwest of the study area, while the weaker radar echoes occur in the northern and northeastern parts of the area (Figure 13d). The clustered stronger radar echoes located in the south and southeast are related to the easterly and the westerly classes, respectively (Figure 13e and 13f). Additionally, the clustered weaker radar echoes located in the northwest and northeast are related to both the easterly and the westerly classes, respectively.

Interestingly, when the data of both classes are combined, the clustered hot spot of strong radar echoes are of a more elongated form and high speed CSs have been observed collocated over the southwest of the study area (Figure 14a and 14b). Detection of these corresponding locations implies the severity of the CS over the study area.

With high statistical significance, 99%, the elliptical shape of MCSs was investigated to better understand the time of occurrence of the more elongated form of MCSs. Most of the CSs were found in all easterly-westerly cases during evening and night time, supported by observations of diurnal variation of propagating convective systems over the tropical land mass by TRMM [27]. Additionally, these clustered CSs are supported by the findings of Satomura [15], in which a mesoscale numerical model was used to simulate diurnal variation of propagating easterly MCSs over the middle of the ICP. Additionally, Takahashi et al. [14] identified a diurnal pattern and also found large quantities of rainfall in the evening and night time over the middle of the ICP. To describe diurnal variation of convective systems, infrared sensors on geostationary satellites were used to detect late night/early morning maximum rainfall over the windward areas of the mountains, basins valleys, and coastal areas [12].

Figure 15 shows a squall line, one of the MCSs types, in the shape of a bow echo propagating over the southwest portion of the radar area. The convective system initiated outside the radar observation range while propagating toward the Dong Phraya range, as shown in Figure 1. While it was propagating, its convective and stratiform cloud areas were enhanced. More elongated forms of the CS shape were detected in the form of squall lines propagating over the radar in both easterly and westerly cases. As discussed by Houze [28], there are four stages of MCS evolution, formative, intensifying, mature and dissipating stages. However, the radar used in this study does not cover a broad enough area to observe all of the MCSs stages. The study of MCS evolution above the landmass of the ICP will be more complete when multiple radar composites are combined the future, similar to research done by Carbone et al. [29] and Carbone and Tuttle [30] using a radar mosaic over the United States.

5. Summary

In order to describe characteristics of the largest convective systems (CSs) during the monsoon march of the rainy season over the middle of Indochina in 2010, a gridded reflectivity was created from instantaneous ground-based radar at Phetchabun, in middle of Thailand. It was done at a height of 3 km using an open source radar library called Wradlib. Additionally, the classification scheme used for the convective region was adopted from Steiner et al. [9] based on a 2D classification background method implemented in a Python environment. The results show that propagating CSs comprise the major population of storms contributing to the total rainfall during the rainy season of the monsoonal march. It was found that in August, the highest number of propagating CSs were associated with relatively larger echo sizes. The classification of directions of the propagating CSs demonstrated that the variation in temporal characteristics

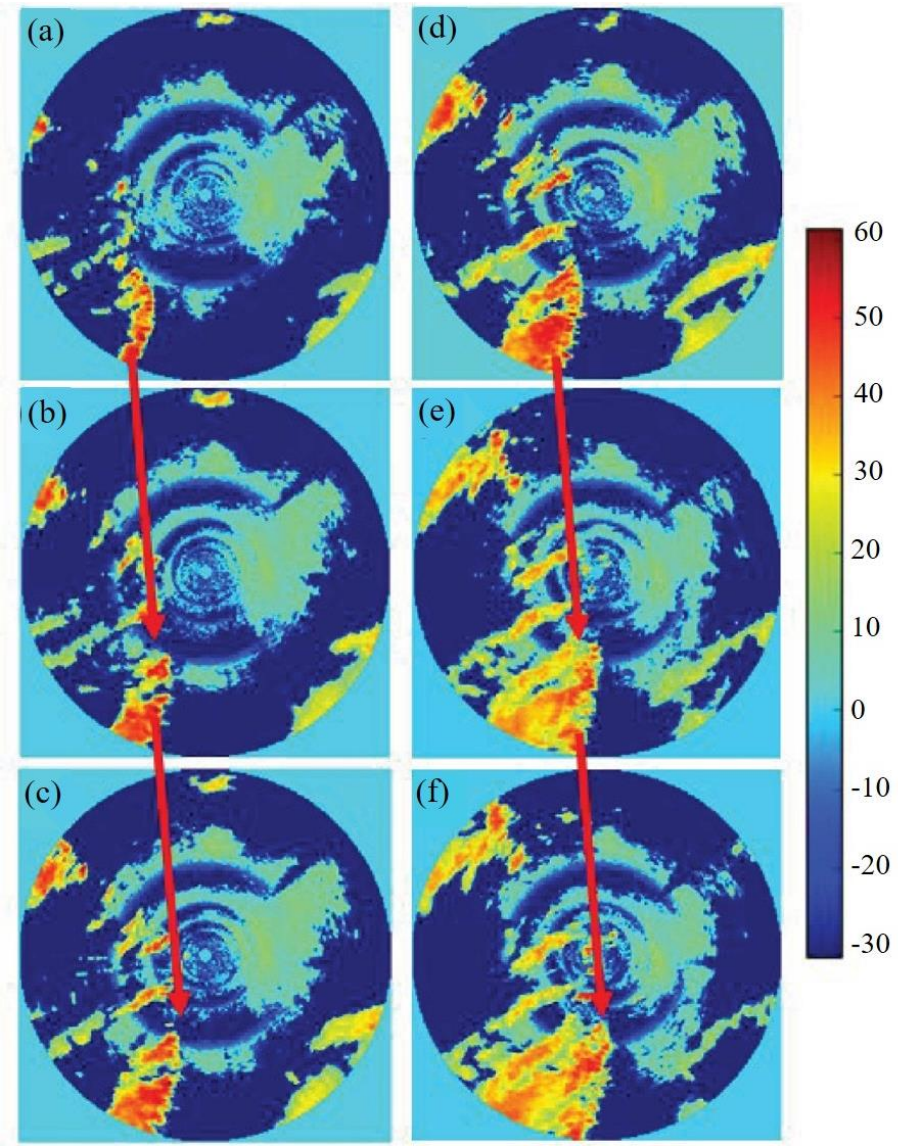

Figure 15 Squall line evolutions during (a-f) at 13:00 - 1445 UTC on 13 August 2010 over the study area (indicated by red arrows) displaying expansion of convective area during dissipation stage of mesoscale convective systems. The color bar indicates radar intensity in dBZ.

was affected by the two prevailing synoptic winds. The speed of the easterly CSs decreased toward the end of the rainy season, while the shape of the system became more elongated. Additionally, larger and stronger echo sizes occurred in August in the case of the westerly class. When considering spatial analysis of the clustered hot spot CSs, the southwest of the study area was identified as producing the most severe propagating CSs based on the collocated area of the easterly and westerly classes.

There were two major limitations in this study. The first limitation was the time span of only three months, which is too short to develop firm conclusions for a climatological study. The second limitation was the small radar observation area, covering only 120 km due to the beam blockage by terrain. Further study should be done to create a radar mosaic using multiple ground-based radar stations to extend the study area for a better understanding of the rain systems and the spatio-temporal characteristics of extreme convective systems. Additionally, inter-seasonal variations of the convective systems should also be investigated.

6. Acknowledgements

This research was supported by National Research Council of Thailand (NRCT) through Naresuan University R2561B062, R2561B063 and R2562B031. We are really appreciate for our project, “Advancing Co-design of Integrated Strategies with Adaptation to Climate Change in Thailand (ADAP-T)” by the Science and Technology Research Partnership for Sustainable Development (SATREPS), and JST-JICA for providing research funds to support the project. The data was supported through project of Integrated Study Project on Hydro-Meteorological Prediction and Adaptation to Climate Change in Thailand (IMPAC-T). Special thanks to the Thai Meteorological Department for providing radar reflectivity data. Additionally, we gratefully thank the developer of

OpenCV and Wradlib libraries for providing the source codes used in Python scripts.

7. References

[1] Pritchard MS, Moncrieff MW, Somerville RC. Orogenic propagating precipitation systems over the United States in a Global Climate Model with embedded explicit convection. J Atmos Sci. 2011;68: 1821-40.

[2] Nesbitt SW, Cifelli R, Rutledge SA. Storm morphology and rainfall characteristics of TRMM precipitation features. Mon Wea Rev. 2006;134:2702-21.

[3] Laing AG, Fritsch JM. The large-scale environments of the global populations of mesoscale convective complexes. Mon Wea Rev. 2000;128:2756-76.

[4] Coniglio MC, Stensrud DJ, Wicker LJ. Effects of upper-level shear on the structure and maintenance of strong quasi-linear mesoscale convective systems. J Atmos Sci. 2006;63:1231-52.

[5] Lang TJ, David AA, Nesbitt SW. Carbone RE. Radar-observed characteristics of precipitating systems during NAME 2004. J Climate. 2007;20:1713-33.

[6] Liu C, Zipser E. Regional variation of morphology of organized convection in the tropics and subtropics. J Geophys Res Atmos, 2013;118:453-66.

[7] Romatschke U, Houze RA. Characteristics of Precipitating Convective Systems in the South Asian Monsoon. J Hydrometeorology. 2011;12:3-26.

[8] Morwal SB, Narkhedkar SG, Padmakumari B, Maheskumar RS, Kulkarni JR. Characteristics of precipitating monsoon clouds over rain-shadow and drought-hit regions of India using radar. Clim Dynam. 2017;9:1-24.

[9] Steiner M, Houze RA, Yuter SE. Climatological characterization of three-dimensional storm structure from operational radar and rain gauge data. J Appl Meteorol. 1995;34:1978-2007.

[10] Xie SP, Xu H, Saji N, Wang Y. Role of narrow mountains in large-scale organization of Asian monsoon convection. J Climate. 2006;19:3420-9.

[11] Matsumoto J. Seasonal transition of summer rainy season over Indochina and adjacent monsoon region. Adv Atmos Sci. 1997;14:231-45.

[12] Ohsawa T, Ueda H, Hayashi T, Watanabe A, Matsumoto J. Diurnal varia-tions of convectivity and rainfall in tropical Asia. J Meteor Soc Japan. 2001;79: 333-52.

[13] Wang B, Ho L. Rainy season of the asian–Pacific summer monsoon. J Climate. 2002;15:386-97.

[14] Takahashi HG, Fujinami H, Yasunari T, Matsumoto J. Diurnal rainfall pattern observed by Tropical Rainfall Measuring Mission Precipitation Radar (TRMM–PR) around the Indochina peninsula. J Geophys Res. 2010;115:1-10.

[15] Satomura T. Diurnal variation of precipitation over the Indo-China Peninsula: two-dimensional numerical simulation. J Meteor Soc Japan. 2000;78:461-75.

[16] Okumura K, Satomura T, Oki T, Khantiyanan W. Diurnal variation of precipitation by moving mesoscale systems: radar observations in northern Thailand. Geophys Res Lett. 2003;30(20):1-5.

[17] Heistermann M, Jacobi S, Pfaff T. Technical note: an open source library for processing weather radar data (wradlib). Hydrol Earth Syst Sci. 2013;17:863-71.

[18] Rigo T, Llasat MC. A methodology for the classification of convective structures using meteorological radar: Application to heavy rainfall events on the Mediterranean coast of the Iberian Peninsula. Nat Hazards Earth Syst Sci. 2004;4:59-68.

[19] Rigo T, Llasat MC. Analysis of mesoscale convective systems in Catalonia using meteorological radar for the period 1996–2000. Atmos Res. 2007;83:458-72.

[20] OpenCV [Internet]. Introduction to OpenCV-Python Tutorials [cited 2019 Jun 23]. Available from https://docs.opencv.org/trunk/d0/de3/tutorial_py_intro.html

[21] Getis A, Ord JK. The Analysis of Spatial Association by Use of Distance Statistics. Geogr Anal. 1992;24(3):189-206.

[22] Satomura T, Yamamoto K, Sysouphanthavong B, Phonevilay S. Diurnal variation of radar echo area in the middle of Indochina. J Meteor Soc Japan. 2011;89A:299-305.

[23] Robinson FJ, Sherwood SC, Gerstle D, Liu C, Kirshbaum DJ. Exploring the land-ocean contrast in convective vigor using Islands. J Atmos Sci 2011;68:602-18.

[24] Takahashi H, Yasunari T. A climatological monsoon break in rainfall over Indochina—A singularity in the seasonal march of the Asian summer monsoon. J Climate. 2006;19:1545-56.

[25] Parker MD, Johnson RH. Simulated convective lines with leading precipitation. part II: evolution and maintenance. J Atmos Sci. 2004;61:1656-73.

[26] Fritsch JM, Murphy RJ, Kain JS. Warm core vortex amplification over land. J Atmos Sci. 1994;51:1781-806.

[27] Johnson RH. Diurnal cycle of monsoon convection. The global monsoon system: research and forecast. Singapore: World Scientific Publishing; 2011.

[28] Houze RA. Cloud Dynamics, 2nd ed. Oxford: Academic Press; 2014.

[29] Carbone RE, Tuttle JD, Ahijevych D, Trier SB. Inferences of predict-ability associated with warm season precipitation episodes. J Atmos Sci. 2002;59: 2033-56.

[30] Carbone RE, Tuttle JD. Rainfall occurrence in the U.S. warm season: the diurnal cycle. J Climate. 2008;21:4132-46.